Nanoscale

RSC Publishing

COMMUNICATION

View Article Online
View Journal | View Issue

Origin of the self-limited electron densities at Al_2O_3/$SrTiO_3$ heterostructures grown by atomic layer deposition – oxygen diffusion model

Cite this: *Nanoscale*, 2013, **5**, 8940

Received 14th June 2013
Accepted 11th August 2013

DOI: 10.1039/c3nr03082b

www.rsc.org/nanoscale

Sang Woon Lee,[a] Jaeyeong Heo[b] and Roy G. Gordon*[a]

Recently, 2-dimensional electron gas (2-DEG) was discovered at the interface of Al_2O_3/$SrTiO_3$ (STO) heterostructures, in which the amorphous Al_2O_3 layers were grown by atomic layer deposition (ALD). The saturated electron density at the Al_2O_3/STO heterostructures above the critical thickness of Al_2O_3 is explained by an oxygen diffusion mechanism.

The observation of 2-dimensional electron gas (2-DEG) was reported at the epitaxial interface of two perovskite-insulators between $LaAlO_3$ (LAO) and $SrTiO_3$ (STO), and it has attracted great interest in oxide electronics.[1,2] It was found that electrons were confined at the interface when an epitaxial-LAO film was grown by pulsed laser deposition (PLD) or molecular beam epitaxy (MBE) on STO substrates.[3–7] These heterostructures were explained by a polar catastrophe mechanism, where the metallic channel was created above the critical thickness of LAO (4 unit cell) film, and the densities of the confined electrons were constant above a critical thickness of the LAO layer.[8] Recently, it was discovered that a 2-DEG can also be created by growing amorphous LAO films on STO substrates, for which the polar catastrophe mechanism does not apply.[9,10] More remarkably, a 2-DEG also formed by growth of amorphous Al_2O_3 films on STO substrates, in which the Al_2O_3 does not have a perovskite-based crystal structure, so no perovskite could be induced in the Al_2O_3 near the substrate.[10]

These amorphous LAO and Al_2O_3 films and the resulting 2-DEG were made by atomic layer deposition (ALD). It is important to note that ALD is widely used to grow functional films of high quality in microelectronic applications, and the ALD process provides great opportunities due to its mass-production compatibility, especially for Al_2O_3 ALD, based on its ideal ALD reaction.[11,12] It turned out that the origin of the formation of 2-DEG using amorphous oxides grown by ALD is the creation of oxygen vacancies in the STO surface, where free electrons are generated. Interestingly, the amorphous Al_2O_3/STO heterostructures also showed a critical thickness of the films for a transition to a metallic interface, and the confined electron densities were constant above the critical thickness of Al_2O_3 layers, although the origin of the carrier generation appears to be completely different from the polar catastrophe of epitaxial LAO/STO heterostructures. The self-limited electron densities at Al_2O_3/STO heterostructures offer great advantages in the control of the electron densities. However, no reason has been proposed for the saturation of the electron density above a critical thickness of the amorphous Al_2O_3 layer. It has been suggested by several researchers that oxygen vacancies generated in the STO substrates are a possible origin of the conductivity induced at the interface during the growth of LAO layers on STO.[13–15] In this communication, the variation of electron density at the interface of the amorphous Al_2O_3/STO heterostructures is explained based on an oxygen diffusion model. It has been proposed that Al_2O_3 layers grown by ALD are highly effective as diffusion barriers and encapsulating layers for many applications.[16–18] Indeed, Al_2O_3 layers deposited on polymer substrates at a low growth temperature (<200 °C) protected them from attack by several gases.[16–18]

Al_2O_3 films were grown on TiO_2-terminated (001) STO single crystals at a growth temperature of 300 °C by ALD at a working pressure of 400 mtorr (base pressure 30 mtorr). Trimethylaluminum (TMA, $Al(CH_3)_3$) was used as the Al-precursor and H_2O was used as the oxygen source for the deposition of Al_2O_3 films. 100 nm-thick Au electrodes (diameter of 1 mm with 10 nm-thick Ti adhesion layer) were deposited at the four corners of the samples for Hall measurements using the van der Pauw configuration. X-ray photoelectron spectroscopy (XPS, K-Alpha, Thermo Scientific) measurements were performed in order to determine the oxidation states of titanium ions near the surface.

[a]*Department of Chemistry and Chemical Biology, Harvard University, Cambridge, Massachusetts 02138, USA. E-mail: gordon@chemistry.harvard.edu; Fax: +1-617-495-4723; Tel: +1-617-496-5393*

[b]*Department of Materials Science and Engineering, Chonnam National University, Gwangju, 500-757, Korea. Fax: +82-62-530-1699; Tel: +82-62-530-1716*

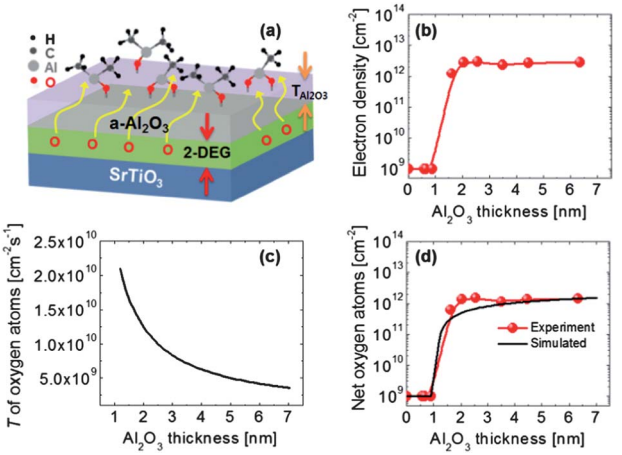

Fig. 1 (a) A schematic of creation mechanism of 2-DEG by the diffused-out oxygen atoms from STO surface through the grown amorphous Al_2O_3 layer by ALD,[10] (b) the variation in the electron densities at Al_2O_3/STO heterostructures depending on the Al_2O_3 film thickness, (c) a transmission rate of oxygen atoms through the Al_2O_3 layer as a function of Al_2O_3 thickness using the value of 2.5×10^{10} oxygen atoms per cm^2 per s at a 1 nm thickness, (d) the number of total oxygen atoms transmitted during Al_2O_3 ALD was calculated using eqn (1), and the experimental curve is obtained by dividing the number of electrons in (b) by 2 (assuming that one oxygen vacancy generates two free electrons).

Fig. 1a shows a schematic of the creation mechanism of 2-DEG by oxygen atoms diffusing out from the STO surface through the amorphous Al_2O_3 layer grown by ALD, as proposed before by our research group.[10] Fig. 1b shows the electron densities obtained by Hall measurement at Al_2O_3/STO interfaces depending on the Al_2O_3 film thickness.[10] The electron densities at Al_2O_3/STO interfaces abruptly increased and then reached a constant electron density of 3×10^{12} cm^{-2} above an Al_2O_3 film thickness of ~1.2 nm. The transition occurs sharply at an Al_2O_3 thickness of 1–2 nm.

The thermodynamic driving force for the out-diffusion of oxygen atoms from the STO is the formation of strong bonds between oxygen and aluminum atoms in TMA molecules chemisorbed onto the surface.[10] The diffusion of oxygen is limited by the growing Al_2O_3 films, because the Al_2O_3 film is a good barrier against diffusion of oxygen atoms.[16,18] It is known that the transmission rate of the oxygen atom through the barrier layer is in inverse proportion to the barrier thickness.[19] Thus, the total oxygen vacancies generated at the STO substrate can be calculated by summation of the oxygen atoms diffusing through the Al_2O_3 layer during the whole Al_2O_3 ALD process above an Al_2O_3 film thickness of ~1.2 nm (14 cycles of Al_2O_3 ALD, which will be discussed below), when the catalytic reduction of STO begins.

It has been reported that the oxygen atoms diffused out from the substrate to the surface due to the concentration gradient of oxygen during the TiO_2 ALD on Ru substrates, which increased the growth rate of the TiO_2 film.[20] In this case, we assumed that oxygen atoms diffuse out from the STO substrate to the surface owing to the thermodynamic potential of TMA for the reduction of STO during TMA pulse.

The ALD process consists of a certain number of ALD cycles.[11] Thus the number of oxygen atoms transmitted from the STO substrate through the growing Al_2O_3 layer may be calculated using the transmission rate and the growth rate of Al_2O_3 film during the ALD process. Fig. 1c shows the transmission rate (T) of oxygen atoms through an Al_2O_3 layer as a function of Al_2O_3 thickness using the value of 2.5×10^{10} oxygen atoms per cm^2 per s at a 1 nm thickness. This value was adopted by fitting the plateau value of the data in Fig. 1d, which results in a permeation rate similar to the literature value.[16] The net oxygen atoms transmitted through the growing Al_2O_3 layer until the Al_2O_3 ALD cycle number becomes x can be estimated by summing the transmission rate of oxygen atoms through each Al_2O_3 layer at every 0.09 nm thickness as below:

$$\sum_{n=14}^{x} T_{1.0}\left(\frac{1}{1.2+0.09(n-14)}\right) \times 3 \text{ s} \quad (1)$$

where $T_{1.0}$ is a transmission rate of oxygen atoms through 1 nm-thick Al_2O_3 layer. This functional form can be estimated from the observed value of 2.5×10^{10} oxygen atoms per cm^2 per s at a 1 nm thickness.[16] The term $1/[1.2 + 0.09(n - 14)]$ indicates the transmission ratio between x nm-thick Al_2O_3 compared to 1 nm-thick Al_2O_3 layer, which is unit-less. The term of 'n' is a cycle number of Al_2O_3 ALD, and a growth rate of Al_2O_3 film at 300 °C is 0.09 nm per cycle, which was extracted from the plot of the Al_2O_3 thickness as a function of ALD cycle number.[10] Here, the injection time of TMA is 3 s during the ALD of Al_2O_3. The calculation of net oxygen atoms transmitted through the growing Al_2O_3 layer were started at $n = 14$ because no reduction of STO happened below $n < 14$ as proved by X-ray photoelectron spectroscopy (XPS) in Fig. 2a.

The XPS result in Fig. 2a indicates that the Ti^{3+} peak (reduction from Ti^{4+}) started to appear at n of 14 (1.2 nm of Al_2O_3 thickness obtained by extrapolation of the Al_2O_3 thickness *vs.* ALD cycle number plot[10]). During the first 13 cycles, the TMA was not effective in reducing Ti and removing oxygen atoms. One possible explanation for this incubation period is that the deposited Al_2O_3 acts as a catalyst for the reduction of STO by TMA. Until sufficient Al_2O_3 catalyst is accumulated on the surface, only a negligible amount of reduction takes place. For films thicker than n of 14, the rate-limiting step in the reduction becomes diffusion through the growing Al_2O_3 film, rather than the catalytic surface reaction. For n of 14 and subsequent cycles, the number of oxygen atoms removed during each ALD Al_2O_3

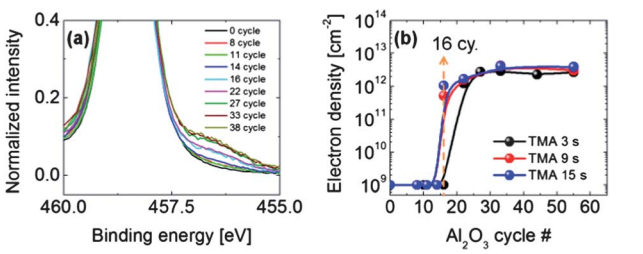

Fig. 2 (a) A normalized XPS spectra of Ti 2p in Al_2O_3/STO heterostructures with increasing n at a given TMA pulse of 3 s, (b) the variation in the electron densities of Al_2O_3/STO heterostructures as a function of Al_2O_3 film thickness for various TMA pulse times.

cycle can thus be calculated using eqn (1) and plotted in Fig. 1d. The simulated result shows a trend similar to the experimentally estimated number of oxygen vacancies. This total number of oxygen vacancies was estimated from the electron densities obtained by Hall measurement, assuming that one oxygen vacancy generates two free electrons and all the oxygen atoms (diffused out) are consumed to oxidize TMA molecules (number of oxygen atoms diffused out is equal to the number of oxygen vacancies at the STO substrate). The simulated curve shows saturation behavior with increasing Al_2O_3 layer thickness because the transmission rate of oxygen atoms quickly decreases with increasing the barrier thickness as shown in Fig. 1c, which results in a self-limited density of oxygen vacancies. Although we cannot determine an exact value of T experimentally, it is now possible to explain why the total number of oxygen atoms diffused out was saturated with increasing Al_2O_3 thickness using a reasonable value of T. Meanwhile, no noticeable change was observed below and above the critical thickness of Al_2O_3 in the XPS spectra of Sr 3d peak.

The self-limited density of oxygen vacancies in Al_2O_3/STO heterostructures is consistent with the XPS result (in Fig. 2a) at a given TMA pulse of 3 s. Fig. 2a shows normalized XPS spectra of Ti 2p in Al_2O_3/STO heterostructures with increasing n at a given TMA pulse of 3 s. The Ti^{3+} peak was not detected until n of 11; however, it started to appear and increased at $n = 14$, and abruptly increased at $n > 16$. The intensity of Ti^{3+} further increased with increasing n, and the intensity was saturated above n of 27 (~2 nm), which is in good agreement with the saturated electron densities as shown in Fig. 1b.

Fig. 2b shows the variation in the electron densities of Al_2O_3/STO heterostructures as a function of n for various TMA pulse times. It should be noted that saturated growth behavior was obtained in the Al_2O_3 ALD with TMA pulse times of 3–15 s due to the self-limiting surface reactions. It appears that the transition n for the creation of electrons was reduced when the injection time of TMA was increased from 3 to 9 and 15 s. Interestingly, the saturated electron densities (3×10^{12} cm^{-2}) above $n > 27$, were not increased further, even though the TMA pulse time was increased from 3 to 15 s. This is because a thicker Al_2O_3 layer is grown by the increased number of reactions between TMA molecules and out-diffusing oxygen atoms from the STO substrate which forms more Al_2O_3, as the TMA pulse time is increased. The thicker Al_2O_3 layer reduces the transmission rate of oxygen atoms, which results in similar electron densities irrespective of TMA pulse time as discussed below.

Fig. 3a–f show the Ti 2p XPS spectra in Al_2O_3/STO heterostructures depending on n for various TMA pulse times. The increment of Ti^{3+} peaks was not noticeable at a n of 8 even though the pulse time of TMA molecules was increased up to 15 s. It was also negligible at a n of 11 with TMA injection of 3 s; however, it was increased substantially with TMA injection of 9 and 15 s. The peaks of Ti^{3+} kept increasing with n up to 22, and the intensity of Ti^{3+} was higher when the TMA injection time was longer. However, it was saturated at a n of 33 irrespective of TMA pulse time, in agreement with the saturated electron densities due to the saturated oxygen vacancies. In other words, although the electrons are created faster in the transition

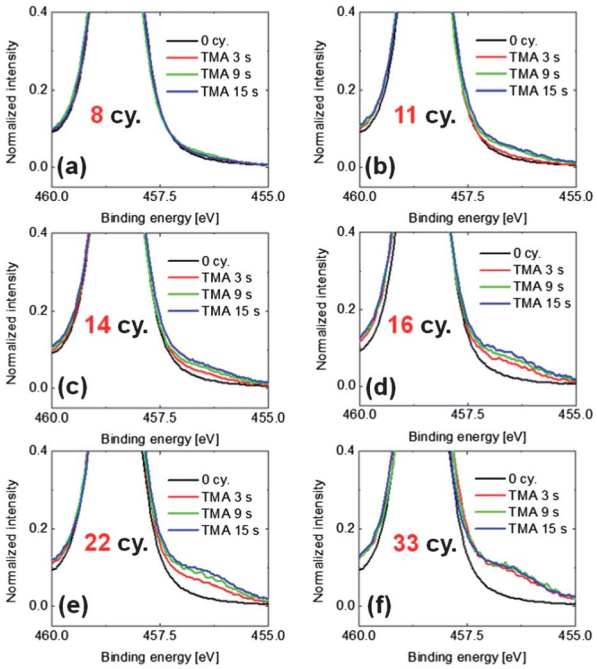

Fig. 3 (a–f) The Ti 2p XPS spectra in Al_2O_3/STO heterostructures depending on n for various TMA pulse times.

regime when the TMA pulse time is long, it reaches the maximum electron densities earlier ($n < 33$) because the transmission rate of oxygen atoms is decreased due to the thicker Al_2O_3 layer by the reaction of oxygen atoms diffusing out with chemisorbed TMA molecules. As a result, the rate of out-diffusion of oxygen atoms slows down by the additionally grown Al_2O_3 layer. It has been reported that metal-oxide films can be grown by oxygen atoms that diffuse out from the substrate during the precursor pulse step.[20,21] Indeed, it was confirmed in our study that more Al_2O_3 film was grown when the TMA pulse is longer even though the n is identical as shown in Fig. 4a, especially for n of 16. Fig. 4a shows the Al 2p XPS spectra of Al_2O_3/STO heterostructures at a n of 16 for various TMA pulse times. The intensity of the Al 2p peak was higher with a longer TMA pulse time, which indicates that a thicker Al_2O_3 film was grown with the increased TMA pulse time. However, the difference in the peak intensities was negligible when the Al_2O_3 layers were grown on silicon substrates where oxygen diffusion does not happen from the silicon substrate, as shown in Fig. 4b

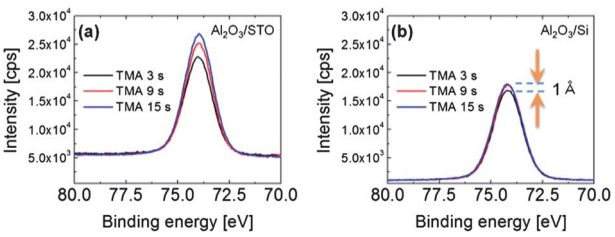

Fig. 4 The Al 2p XPS spectra of (a) Al_2O_3/STO heterostructures and (b) Al_2O_3/Si structures at a n of 16 for various TMA pulse times.

(the difference of the Al_2O_3 film thickness was just 0.1 nm between TMA pulse times of 3 and 15 s, which was determined by ellipsometry).

There is one apparent discrepancy between the electrical measurements and the XPS analysis. For example at *n* of 16, substantial electron densities of $\sim 10^{12}$ cm^{-2} were created with TMA injection times of 9 and 15 s. However, no electrons (below the detection limit of the Hall measurement) were generated with a TMA pulse time of 3 s as shown Fig. 2b, although there is a substantial amount of Ti^{3+} (Fig. 3d). This indicates that a certain minimum amount of Ti^{3+} is needed to achieve a conducting channel, which requires that small oxygen-deficient areas must be sufficiently connected to generate percolation paths of electrons as illustrated in Fig. 5. Unless those areas (which have oxygen vacancies) are sufficiently connected, the lateral resistance must be very high, *i.e.*, the Al_2O_3/STO interface is macroscopically insulating.

It is also important to note that TMA pulses alone (*n* of 16) without introducing any H_2O does not generate Ti^{3+} irrespective of the TMA pulse length. The XPS curves were unchanged when just TMA is pulsed and no water pulses are used (not shown here). This observation may be explained if a critical minimum thickness of the Al_2O_3 layer is necessary to catalyze the reduction of the STO surface. Another limiting factor is that once one monolayer of TMA is adsorbed, no more TMA can be chemisorbed because the surface is covered with non-reactive methyl groups. Further exposures of TMA provide only brief collisions with the surface that do not last long enough for the TMA to react with oxygen in the substrate.

The re-oxidation by H_2O pulse might be possible during the Al_2O_3 ALD. We think that the reduction process by TMA dominates the re-oxidation process by H_2O because a TMA pulse is followed by an H_2O pulse for all the deposition cycles. If the re-oxidation by H_2O were dominant, it would not be possible to observe any oxygen vacancies in the STO substrate even above the critical thickness of Al_2O_3 layer.

In summary, the origin of self-limited saturated electron densities was explained based on a model in which oxygen diffuses out from the STO surface and reacts with chemisorbed TMA on the surface of the growing Al_2O_3 layer. Above an Al_2O_3 layer thickness of $\sim$2 nm grown on a STO substrate, the reduced oxygen transmission rate through the Al_2O_3 layer shuts off further reaction between oxygen diffusing from the STO and chemisorbed TMA. The oxygen vacancies produced near the surface of the STO provide free electrons (about 2 electrons per oxygen vacancy). A 2-DEG is first detected after $\sim$2 nm of Al_2O_3 is deposited. However, reduced titanium ions (Ti^{3+}) detected by XPS provide direct evidence that oxygen has already been removed from the surface of the STO, even when less than 1.5 nm of Al_2O_3 has been deposited without showing macroscopic conductivity. These apparently conflicting observations can be reconciled assuming that only isolated patches of conducting interface are created. Only when the Al_2O_3 thickness reaches $\sim$2 nm do the conducting patches connect together to form percolation paths that provide macroscopic conductivity.

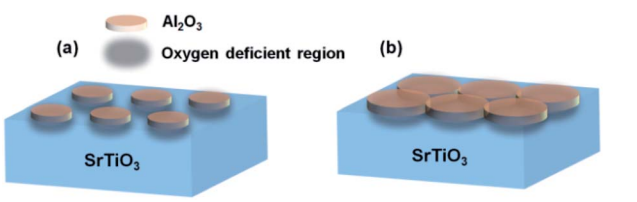

Fig. 5 The illustration of oxygen deficient region in STO substrate in cases of TMA pulse time of (a) 3 s and (b) 15 s at *n* of 16, respectively.

Acknowledgements

The Office of Naval Research (ONR) provided support for this work under contract number ONR N00014-10-1-0937. This work was performed in part at the Center for Nanoscale Systems (CNS) at Harvard University, a member of the National Nanotechnology Infrastructure Network (NNIN), which is supported by the National Science Foundation under NSF award no. ECS-0335765.

References

1 A. Ohtomo and H. Y. Hwang, *Nature*, 2004, **427**, 423–426.
2 J. Mannhart and D. G. Schlom, *Science*, 2010, **327**, 1607–1611.
3 S. Thiel, G. Hammerl, A. Schmehl, C. W. Schneider and J. Mannhart, *Science*, 2006, **313**, 1942–1945.
4 Y. Xie, C. Bell, T. Yajima, Y. Hikita and H. Y. Hwang, *Nano Lett.*, 2010, **10**, 2588–2591.
5 G. Rijnders and D. H. A. Blank, *Nat. Mater.*, 2008, **7**, 270–271.
6 J. W. Park, D. F. Bogorin, C. Cen, D. A. Felker, Y. Zhang, C. T. Nelson, C. W. Bark, C. M. Folkman, X. Q. Pan, M. S. Rzchowski, J. Levy and C. B. Eom, *Nat. Commun.*, 2010, **1**, 94.
7 C. Cen, S. Thiel, G. Hammerl, C. W. Schneider, K. E. Andersen, C. S. Hellberg, J. Mannhart and J. Levy, *Nat. Mater.*, 2008, **7**, 298–302.
8 N. Nakagawa, H. Y. Hwang and D. A. Muller, *Nat. Mater.*, 2006, **5**, 204–209.
9 Y. Chen, N. Pryds, J. e. E. Kleibeuker, G. Koster, J. Sun, E. Stamate, B. Shen, G. Rijnders and S. Linderoth, *Nano Lett.*, 2011, **11**, 3774–3778.
10 S. W. Lee, Y. Liu, J. Heo and R. G. Gordon, *Nano Lett.*, 2012, **12**, 4775–4783.
11 M. Leskelä and M. Ritala, *Angew. Chem., Int. Ed.*, 2003, **42**, 5548–5554.
12 R. L. Puurunen, *J. Appl. Phys.*, 2005, **97**, 121301.
13 G. Herranz, M. Basletić, M. Bibes, C. Carrétéro, E. Tafra, E. Jacquet, K. Bouzehouane, C. Deranlot, A. Hamzić, J. M. Broto, A. Barthélémy and A. Fert, *Phys. Rev. Lett.*, 2007, **98**, 216803.
14 A. Kalabukhov, R. Gunnarsson, J. Börjesson, E. Olsson, T. Claeson and D. Winkler, *Phys. Rev. B: Condens. Matter Mater. Phys.*, 2007, **75**, 121404.
15 W. Siemons, G. Koster, H. Yamamoto, W. A. Harrison, G. Lucovsky, T. H. Geballe, D. H. A. Blank and M. R. Beasley, *Phys. Rev. Lett.*, 2007, **98**, 196802.

16 M. D. Groner, S. M. George, R. S. McLean and P. F. Carcia, *Appl. Phys. Lett.*, 2006, **88**, 051907.
17 P. F. Carcia, R. S. McLean, M. D. Groner, A. A. Dameron and S. M. George, *J. Appl. Phys.*, 2009, **106**, 023533–023536.
18 R. Cooper, H. P. Upadhyaya, T. K. Minton, M. R. Berman, X. Du and S. M. George, *Thin Solid Films*, 2008, **516**, 4036–4039.
19 J. T. Felts, *Proceedings of the Society of Vacuum Coater 36th Annual Technical Conference*, 1991, pp. 99–104.
20 S.-J. Won, S. Suh, S. W. Lee, G.-J. Choi, C. S. Hwang and H. J. Kim, *Electrochem. Solid-State Lett.*, 2010, **13**, G13–G16.
21 S. W. Lee, J. H. Han, S. K. Kim, S. Han, W. Lee and C. S. Hwang, *Chem. Mater.*, 2011, **23**, 976–983.